Short Papers

Coupling Parameters for a Side-Coupled Ring Resonator and a Microstrip Line

Shih-Lin Lu and Altan M. Ferendeci

Abstract—**A ring resonator side coupled to a microstrip line shows two close but distinct resonance peaks. These are identified as due to even-mode (magnetic field) and odd-mode (electric field) coupling. Equivalent circuit models for both cases have been proposed and coupling parameters are calculated using piecewise, coupled-line approximations. The calculated coupling coefficients for the two cases are compared with the experimentally-measured coupling coefficients and show very good agreement with the models used.**

I. Introduction

Among the various applications of ring resonators, they are used to measure dielectric constant of materials [1], to tune and stabilize microwave oscillators [2], and to characterize high temperature superconducting thin films [3]. Ring resonators can be either edge coupled or side coupled to a microstrip transmission line [4]–[6].

Measurements made on side coupled ring resonators show two very close but distinct resonant peaks. The two distinct resonant peaks are identified as the even-mode (magnetic field) and odd-mode (electric field) coupling of the coupled transmission line theory[1] [7].

In this paper, the equivalent circuits for the even- and odd-mode couplings for a ring resonator side coupled to a microstrip line are given and the coupling factor for each case is modeled and calculated using piece-wise coupled-line approximations. The calculated coupling coefficients are found to have very good agreement with the experimentally measured results.

II. Circuit Modeling

Fig. 1 shows a ring resonator side coupled to a microstrip line. The substrate has a thickness h and a relative dielectric constant ε_r. The radii R_2 and R_1 of the ring resonator are chosen for the desired isolated resonance frequency f_o. The microstrip line has a characteristic impedance of $Z_o = 50\,\Omega$. The closest separation distance between the resonator and the microstrip line is d and it is located at a distance D away from the input reference plane.

The lowest order resonant mode of a ring resonator is the TM_{110} mode [8]. The even- and odd-mode couplings take place if the induced magnetic field or the induced electric field is a maximum at the resonator near the microstrip transmission line. As the fields propagate in the microstrip line, the electric and magnetic fields both induce the corresponding electric and magnetic fields in the ring resonator. There results in the ring resonator two simultaneous field distributions with different coupling mechanisms. For the isolated resonator, the resonance frequency of the two modes degenerate into a single mode. When the coupling to the microstrip line takes place, the degeneracy is removed and the double resonance is observed as a result of the different coupling mechanisms associated with the two modes.

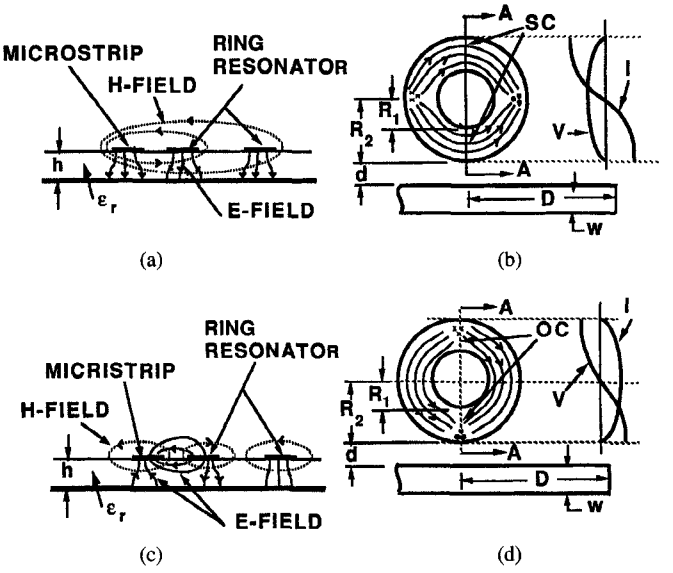

Fig. 1. Ring resonator side coupled to a microstrip line; for the even-mode coupling. (a) Magnetic fields at the plane of d. (b) Corresponding current and voltage distributions; for the odd-mode coupling: (c) Electric fields at the plane d. (b) Corresponding voltage and current distributions.

Fig. 1(a) shows the magnetic fields that couple the microstrip line to the resonator at the plane of the closest distance d. The current distribution is maximum at d and at the farthest and opposite side (at the plane **AA**) as shown in Fig. 1(b). These two planes where the current is a maximum can be thought to be the location of electrical shorts (**SC**). The resulting resonator is then made up of two $\lambda/2$ long short-circuited parallel transmission lines whose lumped equivalent circuit is a series resonant circuit. Coupling to the transmission line is through an ideal transformer with a mutual inductance of M. as shown in Fig. 2(a). This model is equivalent to the even-mode coupling of the coupled transmission line analysis.

For the odd-mode coupling scheme, the induced electric field is maximum at d and also at the opposite end away from d [Fig. 1(c)]. These two extreme planes of the resonator (at the plane **AA**) thus act as electrical open-circuits (**OC**) as shown in Fig. 1(d). The resonator can now be represented by two $\lambda/2$ long open-circuited resonant lines in parallel. These are then equivalent to a parallel resonant circuit coupled to the transmission line through a coupling capacitor C_o as shown in Fig. 2(b).

To calculate the coupling coefficient associated with the even-mode coupling, the equivalent circuit of Fig. 2(a) is used. Here, the loop equations are

$$V_1 = j\omega L_p + j\omega M I_r$$

$$R_r I_r + \frac{1}{j\omega C_r} I_r + j\omega M I_p + j\omega L_r I_r = 0. \tag{1}$$

The subscripts r and p refer respectively to the resonator (secondary) and the primary of the transformer. Solving the set of

Manuscript received June 29, 1994; revised July 18, 1995.

The authors are with the Electrical and Computer Engineering Department, University of Cincinnati, Cincinnati, OH 45221-0030 USA.

Publisher Item Identifier S 0018-9480(96)03785-4.

[1]The even- and odd-mode notation for the coupled lines used here is different than the even and odd integer (n) used to define the simple resonant frequencies of the TM_{n10} mode which relates the mean circumference L to the resonant guide wavelength by $L = n\lambda_g$.

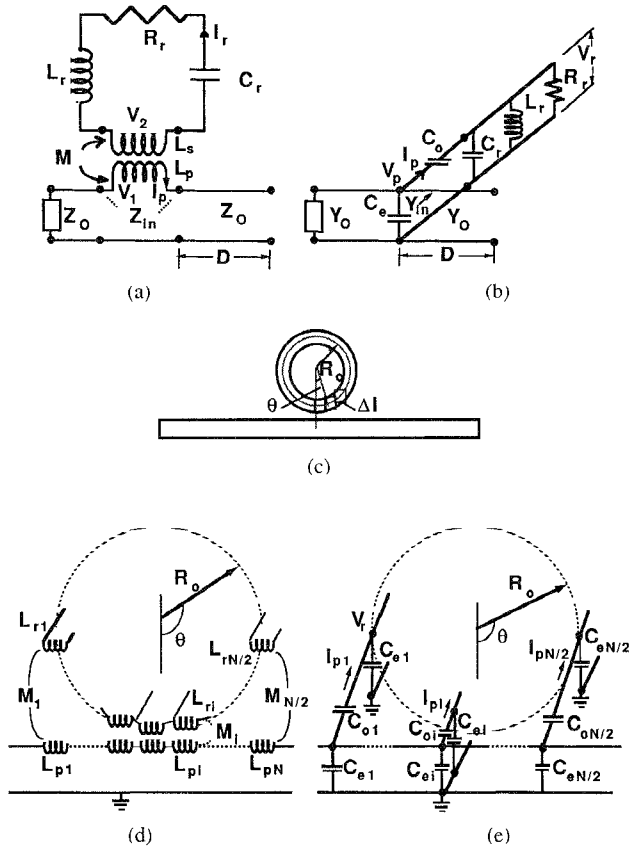

Fig. 2. Equivalent circuits for (a) even-mode and (b) odd-mode coupling. (c) Piece-wise coupled line approximation and the corresponding equivalent circuits used in modeling of the (d) even- and (e) odd-modes.

equation for V_1 in terms of I_p, the input impedance seen at the terminals of the primary can be written as

$$\begin{aligned} Z_{in}^{e} &= \frac{V_1}{I_p} \\ &= j\omega L_p + \frac{\omega^2 M^2}{R_r + j\left(\omega L_r - \frac{1}{\omega C_r}\right)} \\ &\approx \frac{\omega^2 M^2}{R_r + j\left(\omega L_r - \frac{1}{\omega C_r}\right)}. \end{aligned} \tag{2}$$

The term $j\omega L_p$ is small compared to the second term on the right, and is neglected. The circuit given in Fig. 2(a) is thus reflected into the primary of the transformer as an equivalent parallel resonant circuit in series with the transmission line at D.

At D, the input reflection coefficient S_{11}^{e} is

$$S_{11}^{e} = \frac{\frac{Z_{in}^{e}}{2Z_o}}{1 + \frac{Z_{in}^{e}}{2Z_o}}. \tag{3}$$

By definition, the even-mode coupling coefficient is given by $\beta^{e} \equiv Z_{in}^{e}/2Z_o$. The input reflection coefficient at the coupling plane on the line becomes

$$\beta^{e} = \frac{|S_{11}^{e}|}{1 - |S_{11}^{e}|}. \tag{4}$$

Thus, the measurement of the reflection coefficient at resonance provides the coupling coefficient between the ring resonator and the microstrip line.

The odd-mode coupling between the ring resonator and the line can be calculated in a similar way using Fig. 2(b)

$$I_p = j\omega C_o(V_p - V_r)$$

$$G_r V_r + \frac{1}{j\omega L_r} V_r + j\omega C_o(V_r - V_p) + j\omega C_r V_r = 0. \tag{5}$$

The input admittance becomes

$$\begin{aligned} Y_{in}^{o} &= \frac{1}{Z_{in}^{e}} \\ &= \frac{I_p}{V_p} \\ &= j\omega C_o + \frac{\omega^2 C_o^2}{G_r + j\left[\omega(C_r + C_o) - \frac{1}{\omega L_r}\right]}. \end{aligned} \tag{6}$$

The first term is small compared to the second term near resonance and can be neglected. The second term can be represented as a series R_s, L_s, C_s circuit in parallel with the transmission line. Therefore, the two equivalent circuits given in Fig. 2(a) and (b) leads to a phase differences of 180° in S_{11} between the even- and the odd-mode coupling.

By definition, the coupling coefficient for the odd-mode is $\beta^{o} = Y_{in}^{o}/2Y_o$. Again, the measurement of $|S_{11}^{o}|$ at the respective resonant frequency provides the experimental data on the odd-mode coupling coefficient.

III. Computer Simulations

In order to calculate the coupling coefficients for the even- and odd-modes, definition of Q in terms of energy and power loss is used. The external Q of the resonator can be written as

$$Q_e = \frac{\omega W_t}{P_{ex}}. \tag{7}$$

Here W_t is the total stored energy in the resonator and P_{ex} is the power coupled to the external circuit. From Fig. 2(a), for the even-mode these two quantities can be written as

$$\begin{aligned} W_t &= \tfrac{1}{2} L_t I_t^2 \\ P_{ex} &= \frac{|V_1|^2}{4Z_o} \\ &= \frac{(|j\omega M I_r|)^2}{4Z_o} \\ &= \frac{\omega^2 M^2 I_r^2}{4Z_o}. \end{aligned} \tag{8}$$

Here L_r and M are total lumped resonator and mutual inductances.

In order to calculate these quantities, a piece-wise coupled line approximation is made. This is shown in Fig. 2(c) and (d) for the even-mode coupling. The resonator is divided into N segments of length $\Delta l = R_o \Delta\theta$ which are parallel to the main transmission line and are separated by a distance $(d + R_2) - R_2 \cos\theta$. Here $R_o = (R_2 + R_1)/2$ is the mean radius of the ring resonator. Each coupled line segment can be represented by the circuit parameters shown in Fig. 2(d).

Using a current variation of $I \cos\theta$ [4], the total stored energy can be written as

$$\begin{aligned} W_t &= \tfrac{1}{2} L_r I_r^2 \\ &= \tfrac{1}{2} \int_0^{2\pi} L_r (\dot{I} \cos\theta)^2 R_0 \, d\theta. \end{aligned} \tag{9}$$

Here L_r is the distance dependent even-mode inductance associated with the coupled lines.

The coupled power can be written in terms of the voltages generated at each of the primary terminals of the transformers as

$$P_{ex} = \frac{\hat{V}_1^2}{4Z_o} = \frac{(v_1 + v_2 + \cdots + v_N)^2}{4Z_o} = \frac{\left[\sum_{i=1}^{N} \omega M(i)\hat{I} \cos\theta\, \Delta l\right]^2}{4Z_o}. \quad (10)$$

Here $M(i)$ is the distance dependent mutual inductance of the ith line segment.

Finally, the coupling coefficient becomes

$$\beta^e = \frac{Q_o P_{ex}}{\omega W_i} = \frac{Q_o \omega \left[\sum_{i=1}^{N} M(i) \cos\theta\, \Delta l\right]^2}{4Z_o R_0 \int_0^{2\pi} L_r \cos^2\theta\, d\theta}. \quad (11)$$

Here Q_o is the unloaded Q of the resonator.

Similar calculations can be made for the odd-mode coupling. From Fig. 2(b), the total energy stored in the resonator and the power coupled to the external circuit can be written as

$$W_i = \tfrac{1}{2} C_r V_r^2$$
$$P_{ex} = \frac{Z_o}{4} I_p^2. \quad (12)$$

Using the equivalent capacitive transformer, the currents become

$$I_p = j\omega C_o \frac{C_e}{C_e + C_o} V_r. \quad (13)$$

Here the C_o and C_e are odd and even-mode capacitances of the coupled lines.

For the odd-mode coupling, the coupled line approximation leads to the equivalent circuit shown in Fig. 2(e). Using an electric field distribution of $E = E_o \cos\theta$, the total stored energy and the power coupled to the external circuit can be written as

$$W_i = \tfrac{1}{2} C_r V_r^2 = \tfrac{1}{2} \int_0^{2\pi} R_0 C_r (\hat{V} \cos\theta)^2\, d\theta$$
$$P_{ex} = \frac{Z_o}{4} \hat{I}_p^2 = \frac{Z_o}{4} (I_{p1} + I_{p2} + \cdots + I_{pN})^2 \quad (14)$$
$$= \frac{Z_o}{4} \left[\sum_{i=1}^{N} \omega C_o(i) \frac{C_e(i)}{C_o(i) + C_e(i)} \hat{V}_r \cos\theta\, \Delta l\right]^2. \quad (15)$$

Here $C_e(i)$ and $C_o(i)$ are the even and odd-mode capacitances associated with the coupled lines and are functions of the separation distance of the coupled line segments. Finally, the coupling coefficient becomes

$$\beta^o = \frac{Q_o P_{ex}}{\omega W_i} = \frac{Z_o Q_o \omega^2 \left[\sum_{i=1}^{N} \frac{C_o(i) C_e(i)}{C_o(i) + C_e(i)} \cos\theta\, \Delta l\right]^2}{4R_0 \int_0^{2\pi} C_r \cos^2\theta\, d\theta}. \quad (16)$$

Equations (11) and (16) are used to simulate the even- and odd-mode coupling coefficients. For the various distance dependent inductances and capacitances, the corresponding values associated with the even and odd-mode parameters of the coupled-line theory are used [9]. The resulting calculated coupling coefficients for the even- and odd-modes are plotted in Fig. 3 as a function of the separation distance d. For a given separation distance, the coupling coefficient for the even-mode is always higher than the odd-mode coupling.

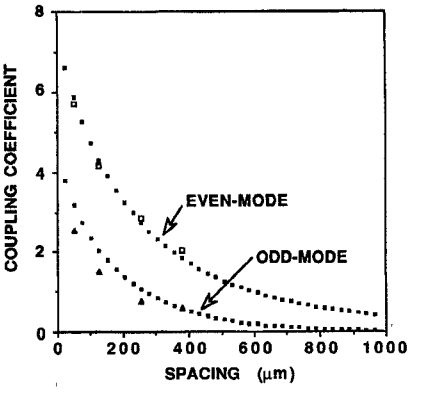

Fig. 3. Calculated coupling coefficients as a function of spacing d for the odd- and even-mode coupling. Experimentally measured odd-mode (△) and even-mode (□) coupling coefficients.

IV. Experimental Results

The coupling parameters for both the even and odd-mode couplings are measured experimentally by preparing various circuits with identical resonator and microstrip dimensions. The only parameter that was different from one circuit to the other was the separation distance d. Alumina having a thickness of 0.508 mm was used as the dielectric substrate. Gold was deposited on both sides of the substrate. Circuits were lithographically processed on one side and the opposite side was used as the ground plane. The microstrip dimensions were chosen to have a characteristic impedance of 50 Ω. The ring resonator dimensions were chosen to have an isolated resonant frequency of 10.4 GHz. 4 circuits with d = 50.8 μm, 125 μm, 254 μm, and 381 μm were prepared.

Using an HP-8510 Vector Network Analyzer, S_{21} were measured over a frequency range of 9.7–11 GHz as shown in Fig. 4. The peaks to the right are due to the even-mode coupling and to the left are due to odd-mode coupling. Using the data in Fig. 4, the even- and odd-mode coupling coefficients β^e and β^o are calculated. These are included in Fig. 3 for comparison with the simulated results. The agreement between the calculated and measured coupling coefficients are very good especially for the even-mode coupling. Even with the approximations made in dividing the ring resonator into lengths $\Delta l = R_o \Delta\theta$ which become zero at $\theta = \pi/2$, most of the contribution to the coupling occurs for distances close to $\theta = 0°$. The odd-mode coupling is lower than the simulated results due to the approximations used in calculating the coupling capacitance values. As the separation distance between the ring resonator and the microstrip line decreases, the incremental coupled line capacitances deviate from the values obtained from the coupled line calculations. E_o which is assumed to be constant varies as a function of the distance between the microstrip line and the ring resonator. These lead to lower capacitance values than the actual capacitances.

Phase difference measurements of S_{11} between the two resonant peaks were also made to enhance the validity of the circuit models for the two coupling modes. For the case of d = 50.8 μm [Fig. 4(a)], the phase difference between the two peaks came out to be 126°. Using the magnitude data, the corresponding inductance, capacitance and resistor values are calculated for each mode. Then, the two circuits

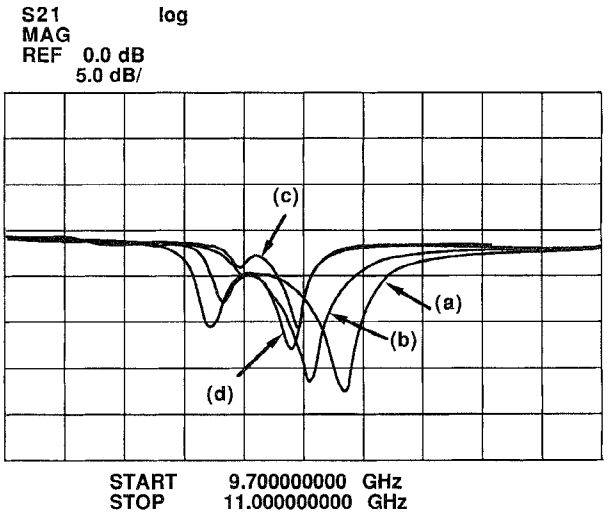

Fig. 4. S21 as a function of frequency for four circuits with identical microstrip and ring resonator dimensions: (R2=2.05 mm, R1=1.58 mm, D=6 35 mm, w=0.470 mm, fo=10 4 GHz, h=0.508 mm) but with different separation distances: (a) d =50.8 μm, (b) d =125 μm (c) d =254 μm, and (d) d =381 μm.

of Fig. 2(a) and (b) are combined to calculate the S_{21} of the overall circuit. For this case, the calculated phase difference came out to be 130° which is very close to the measured value of 126°. Considering the approximations made in determining the circuit elements, the closeness of the measured and calculated phase values also confirms the validity of the even- and odd-mode coupling models presented here.

V. Conclusion

In this paper, the presence of two closely spaced but distinct resonance frequencies of a ring resonator side coupled to a microstrip line are identified as due to the even-mode and odd-mode coupling. The coupling coefficients calculated from the piecewise modeling of the equivalent circuits using the coupled line parameters and the experimentally measured values are in close agreement with each other and verify the presence of the two coupling mechanisms.

References

[1] P. A. Bernard and J. M. Gautray, "Measurement of dielectric constant using a microstrip ring resonator," *IEEE Trans. Microwave Theory Tech.*, vol. 39, p 592, 1991.

[2] S.-L Lu and A M. Ferendeci, "18 GHz hybrid high Tc superconducting microwave oscillator," in *3rd Int. Symp Recent Advances in Microwave Tech (ISRAMT 91)*, Reno, NV, Aug 1991, paper 14.4

[3] J H Takemoto, F. K. Oshita, H. R. Fetterman, P Kobrin, and E. Sovero, "Microstrip ring resonator technique or measuring microwave attenuation in high Tc-superconducting thin films," *IEEE Trans Microwave Theory Tech.*, vol. 37, pp. 1650–1652, 1989

[4] K. Chang, S. Martin, F. Wang, and J. L. Klein, "On the study of microstrip ring and varactor-tuned ring circuits," *IEEE Trans. Microwave Theory Tech.*, vol. MTT-35, pp. 1288–1295, 1987.

[5] T. S. Martin, F. Wang, and K. Chang, "Theoretical and experimental investigation of novel varactor-tuned switchable microstrip ring resonator circuits," *IEEE Trans. Microwave Theory Tech.*, vol. 36, pp. 1733–1739, 1988.

[6] G. K. Gopalakrishnan and K. Chang, "Novel excitation schemes for the microstrip ring resonator with lower insertion loss," *Elect. Lett.*, vol. 30, pp. 148–149, 1994.

[7] S.-L. Lu and A. M. Ferendeci, "Coupling modes of a ring resonator side coupled to a microstrip line," *Electronics Lett.*, vol. 30, p. 1013, 1994.

[8] Y. S. Wu and F. J. Rosenbaum, "Mode chart for microstrip ring resonators," *IEEE Trans. Microwave Theory Tech.*, vol. MTT-21, pp. 487–489, 1973.

[9] R. K. Hoffmann, *Handbook of Microwave Integrated Circuits*. Norwood, MA: Artech House, 1987, ch. 9.

The Use of Active Traveling-Wave Structures in GaAs MMIC's

S. Gareth Ingram and J. Chris Clifton

***Abstract*—A coplanar waveguide has been fabricated on a modulation doped GaAs substrate in order to evaluate the potential of traveling-wave structures in microwave applications. The use of a Schottky contact center conductor enables the line to function as a slow wave structure in which the rf propagation characteristics can be modified with a dc bias. Measurements are reported at 10 GHz on simple structures, some of which incorporated an additional dielectric layer. Results show that slow-wave factors of between 8 and 24 are readily obtained with a loss per slow-wave factor was about 0.7 dB/mm. The practical issues relating to the application of such structures in phase shifters, chip size reduction, compact active filters and resonators are examined.**

I. Introduction

The integration of active traveling-wave structures as planar control components into GaAs monolithic microwave integrated circuits (MMIC's) may provide the means to reduce chip size and increase functionality. At lower frequencies the cost savings could be significant. Traveling-wave structures are transmission line structures which have cross sections analogous to a particular electronic device. The stripline is an example of a nonactive traveling-wave structure, with a cross section based on the parallel plate capacitor. For most purposes, this structure can be considered as a linear transmission line, with propagation properties independent of the rf signal amplitude and any additional dc bias. In contrast, active structures based on junction devices display a marked variation in rf signal propagation with changes in the signal amplitude. For small rf amplitudes, a superimposed dc bias can be used to control the attenuation and electrical length of such a line. Larger signals lead to nonlinear behavior, resulting in pulse shaping, shock wave generation, or even wide-band amplification.

This paper reports on the design and fabrication of Schottky contact transmission lines (SCTL) and metal insulator semiconductor transmission lines (MISTL's) on GaAs to investigate the potential for reducing chip size and for providing voltage-variable signal propagation characteristics.

Manuscript received October 11, 1994, revised February 15, 1996 This work was supported by GEC Marconi Ltd.

S. G. Ingram was with GEC Marconi Materials Technology Ltd., Hirst Division, Borehamwood, Hertfordshire, WD6 IRX, U.K. He is now with DALSA Corp., Waterloo, Ontario, N2V 2E9 Canada.

J. C. Clifton was with GEC Marconi Materials Technology Ltd , Caswell, Towcester, Northants, U.K. He is now with DSC Communications, Ltd. Feltham, Middlesex, U.K.

Publisher Item Identifier S 0018-9480(96)03784-2.